ACS OMEGA

http://pubs.acs.org/journal/acsodf

Article

Solid-Phase Synthesis of Titanium Dioxide Micro-Nanostructures

Xing-hao Han, Chuan-qi Li, Ping Tang, Chen-xiao Feng, Xin-zheng Yue, and Wen-lei Zhang*

Cite This: *ACS Omega* 2022, 7, 35538−35544

Read Online

ACCESS | Metrics & More | Article Recommendations | Supporting Information

ABSTRACT: Titanium dioxide (TiO_2) micro-nanostructures are widely utilized in photochemical applications due to their unique band gaps and are of huge demand in scientific research and industrial manufacture. Herein, this work reports a controllable, facile, economical, and green solid-phase synthesis strategy to prepare TiO_2 with governable morphologies containing 1D nanorods, 3D microbulks, and irregular thick plates. Specifically, Ti powders are transformed into TiO_2 micro-nanostructures through dispersing them into a solid NaOH/KOH mixture with a low eutectic point, followed by grinding, heating, ion exchange, and calcination. As no solvents are utilized in the alkali treatment process, the usage of solvents is decreased and high vapor pressure is avoided. Moreover, the band gaps of TiO_2 micro-nanostructures can be regulated from 3.02 to 3.34 eV through altering the synthetic parameters. Notably, the as-prepared TiO_2 micro-nanostructures exhibit high photocatalytic activities in the degradation of rhodamine B and methylene blue under simulated solar light illumination. It is believed that the solid-phase synthesis strategy will be of huge demand for the synthesis of TiO_2 micro-nanostructures.

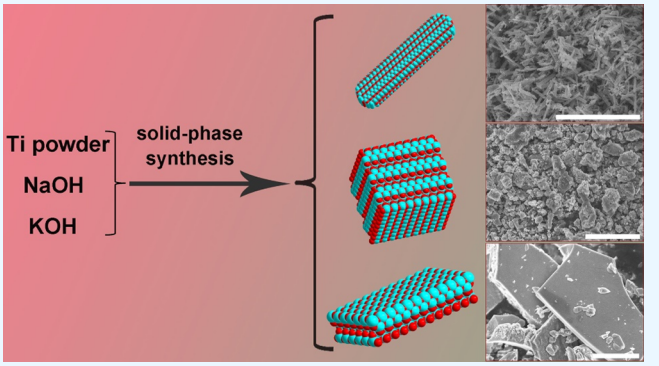

INTRODUCTION

Titanium dioxide (TiO_2) was found to show certain activity in water photolysis reaction in 1972 and has been regarded as a promising and potential photocatalyst by researchers all over the world.[1] In recent years, as a kind of multifunctional semiconductor material, TiO_2 has been extensively investigated by virtue of its potential applications in the fields of lithium-ion batteries,[2,3] dye-sensitized solar cells,[4−6] photocatalytic water splitting,[7,8] degradation of organic compounds,[9,10] and so forth. Compared to other metal oxide micro-nanostructures, TiO_2 micro-nanostructures have attracted much attention due to their excellent photocatalytic activity, high stability, good biocompatibility, and nontoxicity.[11−13] In order to meet various demands for their specific application in different areas, great efforts have been focused on the novel and simple synthesis methods to control the specific morphology and band gap of TiO_2 micro-nanostructures.[14−20]

Notably, it is a generally accepted fact that one-dimensional (1D) semiconductor-based nanostructures could provide large surface areas and well-confined transportation channels for photogenerated charge carriers.[21,22] Therefore, 1D TiO_2 nanostructures usually present a higher photocatalytic activity than other TiO_2 micro-nanostructures (bulks, granular nanoparticles, etc.).[23] In addition, while used as an anode in a lithium-ion battery, 1D TiO_2 nanostructures could not only provide a larger surface area for stronger interface interaction between the electrode and electrolyte and more Li^+ intercalation but also facilitate the conductivity and diffusion of electrons, which results in a high electrochemical performance.[24] Therefore, there is an urgent need to develop controllable, facile, effective, and low-cost approaches to prepare TiO_2 micro-nanostructures, especially 1D TiO_2 nanostructures, such as nanorods (NRs) and nanotubes (NTs).

Various methods have been explored to synthesize 1D TiO_2 nanostructures, such as hydrothermal/solvothermal reaction,[25] electrospinning technique,[26] template method,[27] and so on. However, the inherent disadvantages of these methods limit their practical applications. First, these methods inevitably need organic solvents or water acting as dispersants or templates; thus, large amounts of organic solvents or water are consumed during the reaction process. Second, a high temperature of 150−200 °C should be used with the reaction systems containing water or solvents, which results in increased amounts of energies and production costs. Third, as we know, the abundant dispersants under a high temperature will produce a high vapor pressure, which will improve the possibility of danger in the reaction devices. Therefore, a new green, inexpensive, and safe method should be developed

Received: April 26, 2022
Accepted: September 20, 2022
Published: September 28, 2022

https://doi.org/10.1021/acsomega.2c02591
ACS Omega 2022, 7, 35538−35544

to prepare multifarious TiO_2 micro-nanostructures from the industrial and synthetic points.[28]

Herein, this work reports a new solid-phase synthesis strategy to prepare TiO_2 micro-nanostructures with controllable morphology and adjustable band gaps. Specifically, the TiO_2 micro-nanostructures are prepared through the reaction of Ti powder and solid NaOH/KOH mixture with a low eutectic point and subsequent ion exchange and calcination processes (Figure 1a). No solvents are utilized in the alkali heat

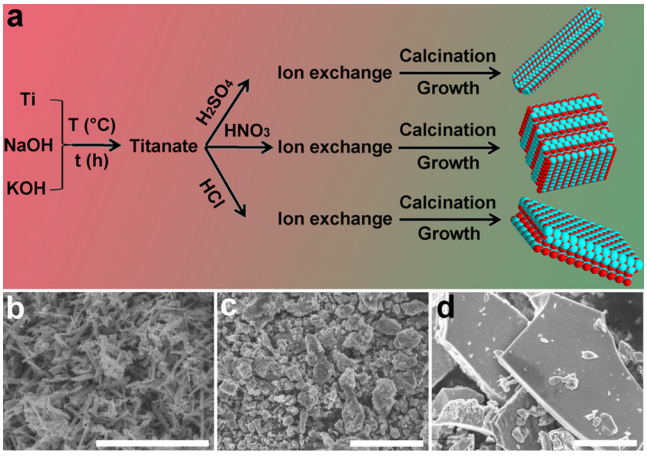

Figure 1. (a) Schematic synthesis process of TiO_2 micro-nanostructures via solid-phase synthesis strategy. SEM images of the synthesized TiO_2 micro-nanostructures, including (b) 1D NRs, (c) 3D microbulks, and (d) irregular thick plates. The scale bars are all 5 μm (b–d).

treatment process, which benefits environmental protection, energy conservation, and safety. The species of inorganic acids utilized in the ion exchange process decide the morphology of the as-prepared TiO_2 micro-nanostructures (dilute H_2SO_4, HNO_3, and HCl, respectively, contribute to 1D NRs, 3D microbulks, and irregular thick plates). Notably, the band gaps of the obtained TiO_2 NRs could be further managed through modifying the experiment parameters. Moreover, the as-prepared TiO_2 samples show high photocatalytic activities for the degradation of rhodamine B (RhB) under simulated solar light irradiation. We believe that this green, economic, and safe solid-phase synthesis strategy will benefit the industrial application of TiO_2 micro-nanostructures.

RESULTS AND DISCUSSION

TiO_2 micro-nanostructures with different dimensionalities are successfully prepared through a solid-phase synthesis strategy (Figure 1b–d). As revealed by the SEM images, the used inorganic acids in the ion exchange process have a crucial impact on the morphology of as-prepared TiO_2 micro-nanostructures. Specifically, the utilized dilute sulfuric acid, dilute nitric acid, and dilute hydrochloric acid, respectively, generate TiO_2 NRs, micro-sized block-shaped powders, and irregular thick plates (Figure S1). Moreover, the morphology of TiO_2 NRs could be further regulated by controlling the reaction time and reaction temperature. Both $P_{t\text{-}18\text{-}S}$ and $P_{t\text{-}36\text{-}S}$ NRs are rods, and their lengths are slightly longer than that of $P_{t\text{-}72\text{-}S}$ NRs (Figure S2a,b). However, they are still inhomogeneous rods with little aggregation. It is noted that the homogeneous and smooth NRs are gradually formed with the increase of reaction temperature, and the length of $P_{T\text{-}220\text{-}S}$ NRs is about 1–1.5 μm (Figure S2c,d), that is, the reaction temperature plays an important role in controlling the morphology of TiO_2 NRs treated by H_2SO_4. The morphology of TiO_2 NRs ($P_{T\text{-}200\text{-}S}$) is further characterized by TEM and HRTEM. It can be clearly observed that the sample is an assembly of uniform long NRs with the length of about 1.3 μm and the diameter of about 8 nm (Figure 2a,b). Additionally, a

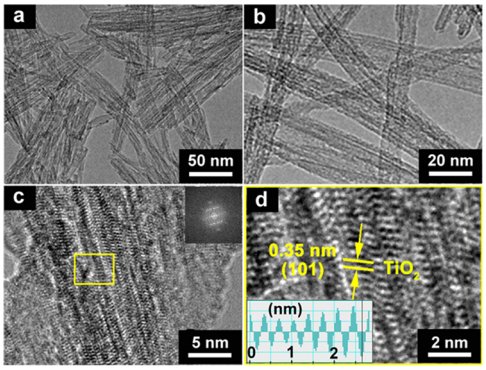

Figure 2. (a) Low- and (b–d) high-resolution TEM images of $P_{T\text{-}200\text{-}S}$ NRs with the corresponding fast Fourier transformation (insert in c) and inverse fast Fourier transformation (insert in d) images.

well-resolved lattice fringe of 0.35 nm corresponding to the (101) plane of TiO_2 is observed (Figure 2c,d). This indicates that 200 °C is the optimum temperature to synthesize TiO_2 NRs in our reaction system.

In addition, XRD characterization is utilized to explore the formation process and crystal structure of the prepared TiO_2 micro-nanostructures. First, the final products achieved through the ion exchange process by H_2SO_4 ($P_{t\text{-}72\text{-}H2SO4}$), HCl ($P_{t\text{-}72\text{-}HCl}$), and HNO_3 ($P_{t\text{-}72\text{-}HNO3}$) all present similar XRD patterns to the anatase phase of TiO_2 (JCPDS 21-1272), while the products untreated by acid ($P_{t\text{-}72\text{-}untreated}$) or treated by H_2O ($P_{t\text{-}72\text{-}H2O}$) show no obvious XRD patterns of the TiO_2 crystal (Figure 3a). In other words, by soaking the amorphous titanate precursor into inorganic acid aqueous solutions, TiO_2 nanostructures with good crystalline property are obtained after the calcination process in air atmosphere. Notably, the XRD patterns of $P_{t\text{-}72\text{-}H2SO4}$, $P_{t\text{-}72\text{-}HCl}$, and $P_{t\text{-}72\text{-}HNO3}$ show significant differences in the intensity of each diffraction peak, which means the kinds of acids have important effects on the crystallization of TiO_2 micro-nanostructures.

To research the formation process of TiO_2 NRs, XRD technology is utilized to monitor the crystal structure of TiO_2 NRs heated at 180 °C for different alkali treatment times of 9, 18, 36, and 72 h ($P_{t\text{-}9\text{-}S}$, $P_{t\text{-}18\text{-}S}$, $P_{t\text{-}36\text{-}S}$, and $P_{t\text{-}72\text{-}S}$). It is clear to see that the intensity of the diffraction peak of Ti powder (about 35.2°) is gradually decreased with the extension of reaction time and disappears while the reaction time reaches 72 h (Figure 3b). This suggests that the alkali treatment time also shows a significant influence on the formation of TiO_2 NRs. In addition, the as-prepared TiO_2 NRs under different alkali treatment temperatures of 180, 200, and 220 °C ($P_{T\text{-}180\text{-}S}$, $P_{T\text{-}200\text{-}S}$, and $P_{T\text{-}220\text{-}S}$) show consistent XRD patterns (Figure S3c), which signify that the reaction temperatures exert little impact on the crystallization of TiO_2 NRs. Moreover, the XRD pattern of the obtained product without adding an alkali into the reaction system ($P_{t\text{-}72\text{-}no\ alkaline\text{-}S}$) shows no obvious diffraction peaks of TiO_2 crystal (Figure S3d), which implies

https://doi.org/10.1021/acsomega.2c02591
ACS Omega 2022, 7, 35538–35544

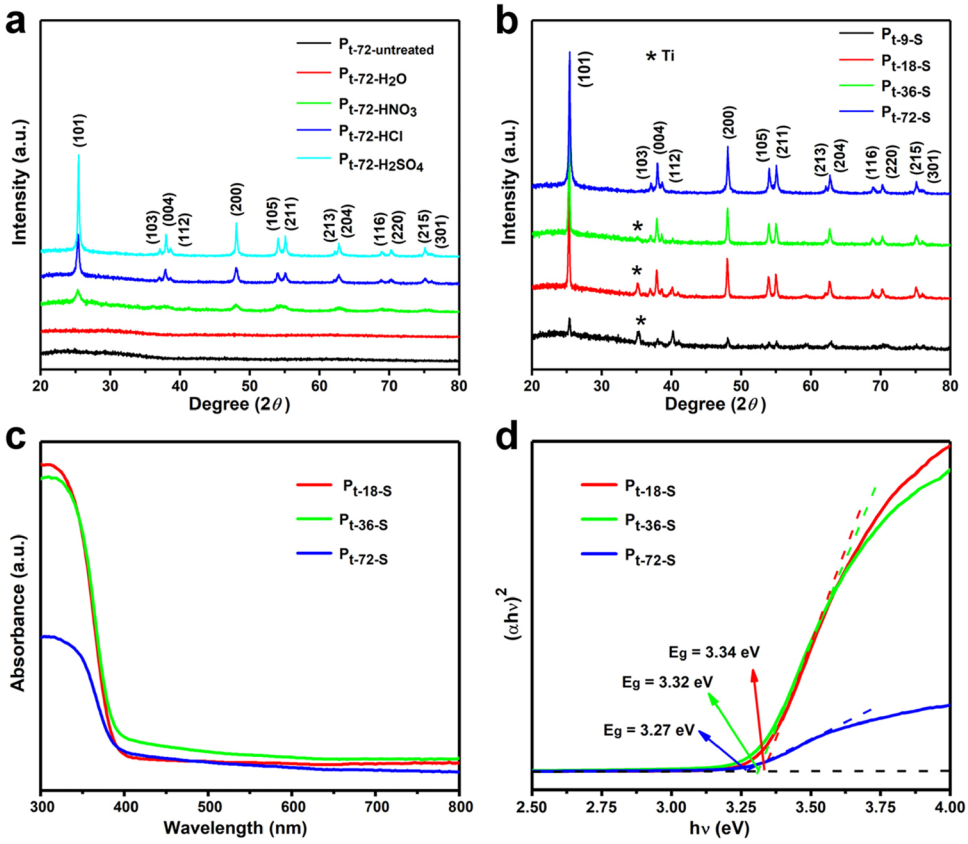

Figure 3. XRD patterns of the TiO_2 micro-nanostructures synthesized under different reaction conditions: (a) treated by different dilute acids in an ion exchange process under reaction time of 72 h; (b) treated by dilute H_2SO_4 in an ion exchange process under different reaction times of 9, 18, 36, and 72 h, respectively. (c) UV−vis DRS of TiO_2 NRs synthesized at different alkali treatment times and (d) corresponding plots of $(\alpha h\nu)^2$ vs photon energy ($h\nu$) for TiO_2 NRs.

the absence of TiO_2 crystal and the essential role of alkali in the formation of TiO_2 NRs.

A comparison of the UV−vis diffuse reflectance spectra (UV−vis DRS) of the TiO_2 micro-nanostructures and their band gaps (E_g) is depicted in Figure S4. Only slight optical property differences are observed among the as-prepared TiO_2 micro-nanostructures treated by different dilute acids, and a red shift of the absorption appears upon the samples of $P_{t\text{-}72\text{-}HCl}$ and $P_{t\text{-}72\text{-}HNO3}$ with respect to $P_{t\text{-}72\text{-}H2SO4}$ (Figure S4a). Besides, it could be clearly observed that not only the alkali treatment times but also the alkali treatment temperatures have influences on the optical properties of the as-prepared TiO_2 NRs (Figures 3c and S4b,c). However, all as-prepared TiO_2 micro-nanostructures show strong absorption at 350 nm, which relates to the electronic excitation from the O 2*p* valence band to Ti 3*d* conduction band.[29] Furthermore, the E_g values of TiO_2 micro-nanostructures are estimated by extrapolating the straight portion of $(\alpha h\nu)^2$ vs photon energy ($h\nu$).[30,31] First, the E_g values of $P_{t\text{-}72\text{-}HNO3}$, $P_{t\text{-}72\text{-}HCl}$, and $P_{t\text{-}72\text{-}H2SO4}$ are, respectively, read to be 3.02, 3.11, and 3.27 eV (Figure S4d), and the difference might be mainly related to the morphology and crystallinity of the synthesized TiO_2 micro-nanostructures. Second, the E_g values of $P_{t\text{-}18\text{-}S}$, $P_{t\text{-}36\text{-}S}$, and $P_{t\text{-}72\text{-}S}$ NRs are, respectively, read to be 3.34, 3.32, and 3.27 eV (Figure 3d), and the slight difference should be mainly ascribed to the contents of metallic Ti in the obtained products. At last, the E_g values of $P_{T\text{-}180\text{-}S}$, $P_{T\text{-}200\text{-}S}$, and $P_{T\text{-}220\text{-}S}$ NRs are, respectively, read to be 3.27, 3.27, and 3.31 eV (Figure S4f), and the slight difference should be attributed to the crystal structure of the obtained TiO_2 NRs.

In addition, the growth mechanism of TiO_2 micro-nanostructures is also explored and revealed. It is reported that the melting points of pure NaOH and KOH are, respectively, 323 and 360 °C, while the eutectic point of NaOH/KOH (mass ratio = 51.5:48.5) is only about 165 °C.[32] After grinding and heating the mixture of Ti powder, NaOH, and KOH, the TiO_2 precursor (titanate) is formed according to the following eq 1:[33]

$$2Ti + 2NaOH + 2KOH + 2O_2 \rightarrow Na_2TiO_3 + K_2TiO_3 + 2H_2O \quad (1)$$

Then, the titanate precursor is transformed into titanic acid after the ion exchange process according to the following eqs 2 and 3:[34]

$$Na_2TiO_3 + 2HX \rightarrow H_2TiO_3 + 2NaX \text{ (Room condition)} \quad (2)$$

$$K_2TiO_3 + 2HX \rightarrow H_2TiO_3 + 2KX \text{ (Room condition)} \quad (3)$$

where HX represents inorganic acids. In order to prove that the precursors of the ion exchange process are Na_2TiO_3 and K_2TiO_3, the inductive coupled plasma emission spectrometry (ICP) measurements are utilized to quantify the alkali metal in the obtained precursors. Clearly, the measured concentrations of Na^+ and K^+ increase with the time of ion exchange process,

https://doi.org/10.1021/acsomega.2c02591
ACS Omega 2022, 7, 35538−35544

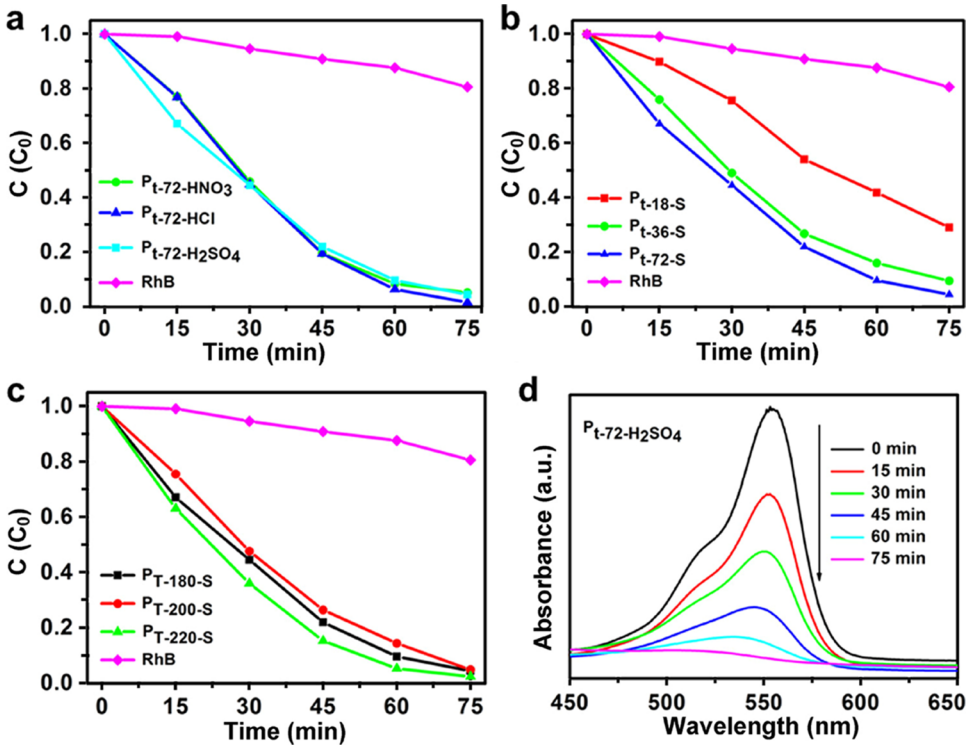

Figure 4. (a–c) Photocatalytic degradation of RhB over different TiO_2 micro-nanostructures; (d) UV–vis absorption spectra during the photocatalytic degradation of RhB in aqueous solution in the presence of $P_{t\text{-}72\text{-}H2SO4}$ NRs.

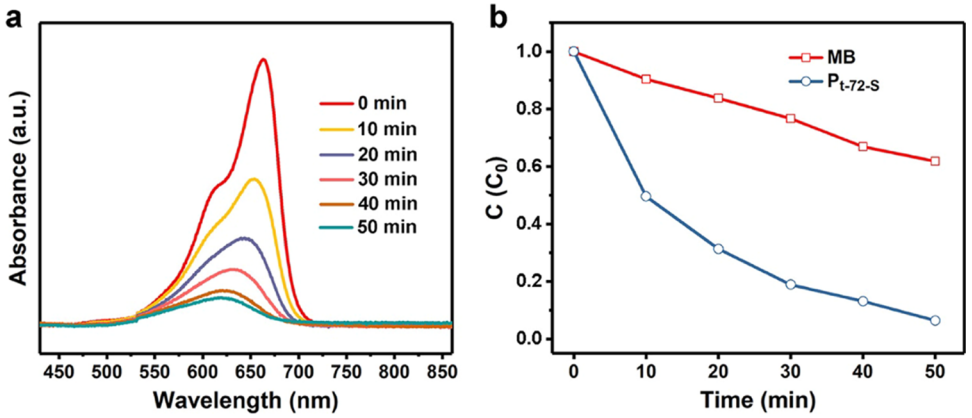

Figure 5. (a) UV–vis absorption spectra and (b) photocatalytic degradation activity during the photocatalytic degradation of MB over $P_{t\text{-}72\text{-}S}$ nanostructures.

and the ICP results can confirm well the reaction theory listed in eqs 1–3 (Table S2).

Finally, the titanate is transformed into $H_2Ti_2O_3$ through the ion exchange process, and TiO_2 powder could be obtained when $H_2Ti_2O_3$ is sintered at 450 °C for 2 h, as in the eq 4:[35]

$$H_2TiO_3 \rightarrow TiO_2 + H_2O \quad (4)$$

For comparing and analyzing the influence of acids ultimately, H_2O is used to replace the HNO_3 solution to conduct the ICP experiment (3 h), and the results show low concentrations of Na^+ (1.65 mmol L^{-1}) and K^+ (1.10 mmol L^{-1}), which should be attributed to the low solubility of Na_2TiO_3 and K_2TiO_3 in H_2O.

The degradation of organic contaminants has always been a research emphasis in the photocatalytic field.[36,37] Herein, the photocatalytic activities of the as-prepared TiO_2 micro-nanostructures are first evaluated by degrading the organic contaminant rhodamine B (RhB) in aqueous solution under simulated solar light irradiation. It is obviously observed that all TiO_2 micro-nanostructures prepared by different acids exhibit high photocatalytic activities (Figure 4a), signifying that the morphology of TiO_2 nanostructures exerts a slight influence on their photocatalytic activities. Moreover, TiO_2 NRs prepared by dilute H_2SO_4 under different reaction times present an ordered activity: $P_{t\text{-}18\text{-}S} < P_{t\text{-}36\text{-}S} < P_{t\text{-}72\text{-}S}$ (Figure 4b), which should be ascribed to their different E_g values and Ti contents. In addition, due to similar E_g values, there are almost no variations in the degradation of RhB in the presence of TiO_2 NRs obtained under different alkali treatment temperatures, as shown in Figure 4c. The absorption spectra of RhB degradation over $P_{t\text{-}72\text{-}H2SO4}$ NRs are shown in Figure 4d. During the photocatalytic degradation process, the absorption

https://doi.org/10.1021/acsomega.2c02591
ACS Omega 2022, 7, 35538–35544

peak at about 554 nm is significantly decreased, and about 96% of RhB is degraded after 75 min. Furthermore, the as-prepared TiO_2 NRs also show an obvious activity in the photocatalytic degradation of methylene blue (MB) (Figure 5). In a word, the prepared TiO_2 micro-nanostructures possess high photocatalytic activities.

CONCLUSIONS

In conclusion, we have successfully synthesized 1D nanorods, 3D microbulks, and irregular thick plates via a solid-phase synthesis strategy. No solvents are utilized in the alkali treatment process under high temperatures, which avoids high vapor pressures and decreases the usage of solvents. In addition, the morphology of TiO_2 micro-nanostructures could be tuned by treating the titanate precursor with different acids in the ion exchange process, and the E_g values of TiO_2 micro-nanostructures could also be precisely regulated through altering the synthetic parameters. Moreover, the as-prepared TiO_2 samples exhibit high photocatalytic activities in the degradation of organic contaminants under simulated solar light illumination. In short, the solid-phase synthesis strategy provides a controllable, facile, economical, and green platform for the synthesis of TiO_2 micro-nanostructures.

EXPERIMENTAL SECTION

Materials. All chemicals are analytical grade reagents and are used as received without further purification. Potassium hydroxide (KOH, ≥90%), sodium hydroxide (NaOH, ≥96%), sulfuric acid (H_2SO_4, 98.3%), hydrochloric acid (HCl, 38%), and nitric acid (HNO_3, 68%) are purchased from Beijing Chemical Works. Ti powder (~100 mesh) is purchased from Aladdin Reagent Co., Ltd. Deionized water with a specific resistance of 18.2 MΩ cm is obtained by reverse osmosis, followed by ion exchange and filtration.

Synthesis of TiO_2 NRs ($P_{t\text{-}72\text{-}H2SO4}$). In a typical synthesis, 1.5 g of Ti powder, 6.18 g of NaOH, and 5.82 g of KOH are poured into an agate mortar. After being grinded for about 15 min, the mixture is loaded into a 50-mL Teflon-lined autoclave and heated at 180 °C for 72 h. When it is allowed to cool to room temperature, the precipitates are collected and fully washed with deionized water until pH = 7. Next, the obtained products are soaked in dilute H_2SO_4 (volume ratio of H_2O to H_2SO_4 is 5:1) for 2 h. After that, the obtained precipitates are centrifuged and washed with deionized water and ethanol several times and dried at 80 °C for 12 h. Finally, TiO_2 could be achieved by sintering at 450 °C for 2 h in air atmosphere with a heating rate of 5 °C min^{-1}. As a result, the sample is denoted as $P_{t\text{-}72\text{-}H2SO4}$ (or $P_{t\text{-}72\text{-}S}$).

Synthesis of Other TiO_2 Micro-Nanostructures. In order to explore the influence of various acids on the final products of TiO_2, parallel experiments are conducted by, respectively, choosing HCl, HNO_3, and H_2O to treat the titanate precursor. The resultant specimens are denoted as $P_{t\text{-}72\text{-}HCl}$, $P_{t\text{-}72\text{-}HNO3}$, and $P_{t\text{-}72\text{-}H2O}$, respectively. Furthermore, in order to investigate the influence of the alkali treatment time (t) on the final TiO_2 NRs, the experiments occurred at other times (9, 18, and 36 h) are carried out, and the as-prepared TiO_2 NRs are denoted as $P_{t\text{-}9\text{-}S}$, $P_{t\text{-}18\text{-}S}$, and $P_{t\text{-}36\text{-}S}$, respectively. Similarly, we fixed the alkali treatment time of 72 h and changed the reaction temperatures (T) of 180, 200, and 220 °C, respectively, and the final NRs of TiO_2 alkali treatment are marked as $P_{T\text{-}180\text{-}S}$, $P_{T\text{-}200\text{-}S}$, and $P_{T\text{-}220\text{-}S}$. As a comparison, the same conditions as that of $P_{t\text{-}72\text{-}S}$ were maintained, except removing the alkali compound in the preparation process of the titanate precursor, and the obtained final product is denoted as $P_{t\text{-}72\text{-}noalkali\text{-}S}$.

Characterizations. The crystalline phase is determined by XRD with a Rigaku D/Max-2550 diffractometer using Cu Kα radiation (λ = 1.541 nm Å) at 50 kV and 200 mA in the 2θ range of 20−80° at a scanning rate of 10° min^{-1}. The UV−vis DRS spectra are measured on dispersions using a UV−vis−NIR spectrophotometer (Shimadzu UV-3600) to detect absorption over the range 300−800 nm. The FESEM images are obtained on a field emission scanning electron microscope (JSM-6700F, Japan). The TEM and HRTEM images are obtained on a TECNAIG TEM microscope (FEI Company).

Photocatalytic Experiment. The photocatalytic degradation efficiency of RhB is assessed in a cylindrical Pyrex flask (50 mL) at room temperature. A 500 W Xenon lamp (CHFXQ 500 W, Global Xenon Lamp Power) is employed as the simulated solar light source. Initially, 20 mL of the aqueous dye solution (10 mg L^{-1}) and 20 mg of the photocatalyst are put into the reactor, sonicated for 5 min, and continuously stirred for 1 h in the dark to ensure the establishment of the adsorption−desorption equilibrium of RhB molecules on the surface of the photocatalyst before illumination. The analytical solution is taken from the suspension at intervals of 15 min under solar light irradiation and then immediately centrifuged at 10,000 rpm for 5 min. The photocatalytic degradation efficiency is detected by measuring the absorption at 554 nm of RhB, using a UV−vis spectrometer (Maya 2000 Pro) at room temperature. The photocatalytic degradation of MB is conducted under similar conditions, except dispersing 50 mg of catalysts into 150 mL of MB aqueous solution.

ASSOCIATED CONTENT

Supporting Information

The Supporting Information is available free of charge at https://pubs.acs.org/doi/10.1021/acsomega.2c02591.

Experimental section, SEM, XRD, UV−vis DRS, and ICP data (PDF)

AUTHOR INFORMATION

Corresponding Author

Wen-lei Zhang − *College of Chemistry, Green Catalysis Center, Henan Institutes of Advanced Technology, Zhengzhou University, Zhengzhou 450001, China;* orcid.org/0000-0002-2790-6107; Email: wenleizhang@zzu.edu.cn

Authors

Xing-hao Han − *Public Teaching Department, Tibet Agriculture and Animal Husbandry University, Nyingchi 860000, China; College of Chemistry, Green Catalysis Center, Henan Institutes of Advanced Technology, Zhengzhou University, Zhengzhou 450001, China*

Chuan-qi Li − *College of Chemistry, Green Catalysis Center, Henan Institutes of Advanced Technology, Zhengzhou University, Zhengzhou 450001, China*

Ping Tang − *College of Chemistry, Green Catalysis Center, Henan Institutes of Advanced Technology, Zhengzhou University, Zhengzhou 450001, China*

https://doi.org/10.1021/acsomega.2c02591
ACS Omega 2022, 7, 35538−35544

Chen-xiao Feng − *College of Chemistry, Green Catalysis Center, Henan Institutes of Advanced Technology, Zhengzhou University, Zhengzhou 450001, China*

Xin-zheng Yue − *College of Chemistry, Green Catalysis Center, Henan Institutes of Advanced Technology, Zhengzhou University, Zhengzhou 450001, China;* orcid.org/0000-0002-8758-9246

Complete contact information is available at: https://pubs.acs.org/10.1021/acsomega.2c02591

Notes

The authors declare no competing financial interest.

■ ACKNOWLEDGMENTS

This work was supported by a postdoctoral fellowship of Zhengzhou University.

■ REFERENCES

(1) Fujishima, A.; Honda, K. Electrochemical photolysis of water at a semiconductor electrode. *Nature* **1972**, *238*, 37−38.

(2) Ren, H.; Yu, R.; Qi, J.; Zhang, L.; Jin, Q.; Wang, D. Hollow Multishelled Heterostructured Anatase/TiO_2(B) with Superior Rate Capability and Cycling Performance. *Adv. Mater.* **2019**, *31*, No. e1805754.

(3) Wang, N.; Chu, C.; Xu, X.; Du, Y.; Yang, J.; Bai, Z.; Dou, S. Comprehensive New Insights and Perspectives into Ti-Based Anodes for Next-Generation Alkaline Metal (Na^+, K^+) Ion Batteries. *Adv. Energy Mater.* **2018**, *8*, No. 1801888.

(4) Sokoll, K. S.; Robinson, W. E.; Warnan, J.; Kornienko, N.; Nowaczyk, M. M.; Ruff, A.; Zhang, J. Z.; Reisner, E. Bias-Free Photoelectrochemical Water Splitting with Photosystem II on a Dye-Sensitized Photoanode Wired to Hydrogenase. *Nat. Energy* **2018**, *3*, 944−951.

(5) Cao, Y.; Liu, Y.; Zakeeruddin, S. M.; Hagfeldt, A.; Grätzel, M. Direct Contact of Selective Charge Extraction Layers Enables High-Efficiency Molecular Photovoltaics. *Joule* **2018**, *2*, 1108−1117.

(6) Hu, K.; Sampaio, R. N.; Schneider, J.; Troian-Gautier, L.; Meyer, G. J. Perspectives on Dye Sensitization of Nanocrystalline Mesoporous Thin Films. *J. Am. Chem. Soc.* **2020**, *142*, 16099−16116.

(7) Guo, Q.; Ma, Z.; Zhou, C.; Ren, Z.; Yang, X. Single Molecule Photocatalysis on TiO_2 Surfaces. *Chem. Rev.* **2019**, *119*, 11020−11041.

(8) Gao, C.; Wei, T.; Zhang, Y.; Song, X.; Huan, Y.; Liu, H.; Zhao, M.; Yu, J.; Chen, X. A Photoresponsive Rutile TiO_2 Heterojunction with Enhanced Electron−Hole Separation for High-Performance Hydrogen Evolution. *Adv. Mater.* **2019**, *31*, No. 1806596.

(9) Wang, D.; Li, Q.; Miao, W.; Liu, Y.; Du, N.; Mao, S. One-pot Synthesis of Ultrafine NiO Loaded and Ti^{3+} in-situ Doped TiO_2 Induced by Cyclodextrin for Efficient Visible-Light Photodegradation of Hydrophobic Pollutants. *Chem. Eng. J.* **2020**, *402*, No. 126211.

(10) Jiang, D.; Otitoju, T. A.; Ouyang, Y.; Shoparwe, N. F.; Wang, S.; Zhang, A.; Li, S. A Review on Metal Ions Modified TiO_2 for Photocatalytic Degradation of Organic Pollutants. *Catalysts* **2021**, *11*, 1039.

(11) Ansari, S. A.; Khan, M. M.; Ansari, M. O.; Cho, M. H. Nitrogen-doped Titanium Dioxide (N-doped TiO2) for Visible Light Photocatalysis. *New J. Chem.* **2016**, *40*, 3000−3009.

(12) Li, Z.; Li, Z.; Zuo, C.; Fang, X. Application of Nanostructured TiO_2 in UV Photodetectors: A Review. *Adv. Mater.* **2022**, *34*, No. 2109083.

(13) Lan, K.; Wei, Q.; Zhao, D. Versatile Synthesis of Mesoporous Crystalline TiO_2 Materials by Monomicelle Assembly. *Angew. Chem. Int. Ed. Engl.* **2022**, *61*, No. e2022007.

(14) Yang, G.; Yan, Z.; Xiao, T.; Yang, B. Low-Temperature Synthesis of Alkalis Doped TiO_2 Photocatalysts and Their Photocatalytic Performance for Degradation of Methyl Orange. *J. Alloys Compd.* **2013**, *580*, 15−22.

(15) Si, L.; Huang, Z.; Lv, K.; Ye, H.; Deng, K.; Wu, Y. Fabrication of TiO_2 Hollow Microspheres by Ammonia-Induced Self-Transformation. *J. Alloys Compd.* **2014**, *612*, 69−73.

(16) Peng, X.; Chen, A. Large-Scale Synthesis and Characterization of TiO_2-Based Nanostructures on Ti Substrates. *Adv. Funct. Mater.* **2006**, *16*, 1355−1362.

(17) Hosono, E.; Fujihara, S.; Imai, H.; Honma, I.; Masaki, I.; Zhou, H. One-Step Synthesis of Nano−Micro Chestnut TiO_2 with Rutile Nanopins on the Microanatase Octahedron. *ACS Nano* **2007**, *1*, 273−278.

(18) Calisir, M. D.; Gungor, M.; Demir, A.; Kilic, A.; Khan, M. M. Nitrogen-doped TiO_2 Fibers for Visible-Light-Induced Photocatalytic Activities. *Ceram. Int.* **2020**, *46*, 16743−16753.

(19) Khan, M. E.; Khan, M. M.; Min, B.-K.; Cho, M. H. Microbial Fuel Cell Assisted Band Gap Narrowed TiO2 for Visible Light-Induced Photocatalytic Activities and Power Generation. *Sci. Rep.* **2018**, *8*, 1723.

(20) Khan, M. M.; Ansari, S. A.; Pradhan, D.; Ansari, M. O.; Han, D. H.; Lee, J.; Cho, M. H. Band Gap Engineered TiO2 Nanoparticles for Visible Light Induced Photoelectrochemical and Photocatalytic Studies. *J. Mater. Chem. A* **2014**, *2*, 637−644.

(21) Wu, K.; Lian, T. Quantum Confined Colloidal Nanorod Heterostructures for Solar-to-Fuel Conversion. *Chem. Soc. Rev.* **2016**, *45*, 3781−3810.

(22) Yi, S. S.; Yan, J. M.; Wulan, B. R.; Jiang, Q. Efficient Visible-Light-Driven Hydrogen Generation from Water Splitting Catalyzed by Highly Stable CdS@Mo_2C-C Core−Shell Nanorods. *J. Mater. Chem. A* **2017**, *5*, 15862−15868.

(23) Tian, J.; Zhao, Z.; Kumar, A.; Boughtonc, R. I.; Liu, H. Recent Progress in Design, Synthesis, and Applications of One-Dimensional TiO_2 Nanostructured Surface Heterostructures: A Review. *Chem. Soc. Rev.* **2014**, *43*, 6920−6937.

(24) Paul, S.; Rahman, M. A.; Sharif, S. B.; Kim, J.-H.; Siddiqui, S.-E.-T.; Hossain, M. A. M. TiO_2 as an Anode of High-Performance Lithium-Ion Batteries: A Comprehensive Review towards Practical Application. *Nanomaterials* **2022**, *12*, 2034.

(25) Ding, J.; Wang, L.; Zhao, Y.; Xing, L.; Yu, X.; Chen, G.; Zhang, J.; Che, R. Boosted Interfacial Polarization from Multishell TiO_2@Fe_3O_4@PPy Heterojunction for Enhanced Microwave Absorption. *Small* **2019**, *15*, No. 1902885.

(26) Xu, F.; Meng, K.; Cao, S.; Jiang, C.; Chen, T.; Xu, J.; Yu, J. Step-by-Step Mechanism Insights into the TiO_2/Ce_2S_3 S-Scheme Photocatalyst for Enhanced Aniline Production with Water as a Proton Source. *ACS Catal.* **2022**, *12*, 164−172.

(27) Xu, T.; Liu, X.; Wang, S.; Li, L. Ferroelectric Oxide Nanocomposites with Trimodal Pore Structure for High Photocatalytic Performance. *Nano-Micro Lett.* **2019**, *11*, 37.

(28) Khan, M. M.; Adil, S. F.; Al-Mayouf, A. Metal Oxides as Photocatalysts. *J. Saudi Chem. Soc.* **2015**, *19*, 462−464.

(29) Umebayashi, T.; Yamaki, T.; Itoh, H.; Asai, K. Band Gap Narrowing of Titanium Dioxide by Sulfur Doping. *Appl. Phys. Lett.* **2002**, *81*, 454−456.

(30) Yue, X.; Yi, S.; Wang, R.; Zhang, Z.; Qiu, S. Cobalt Phosphide Modified Titanium Oxide Nanophotocatalysts with Significantly Enhanced Photocatalytic Hydrogen Evolution from Water Splitting. *Small* **2017**, *13*, No. 1603301.

(31) Yue, X.; Yi, S.; Wang, R.; Zhang, Z.; Qiu, S. A Novel and Highly Efficient Earth-Abundant Cu_3P with TiO_2 ″p-n″ Heterojunction Nanophotocatalyst for Hydrogen Evolution from Water. *Nanoscale* **2016**, *8*, 17516−17523.

(32) Liu, H.; Hu, C.; Wang, Z. L. Composite-Hydroxide-Mediated Approach for the Synthesis of Nanostructures of Complex Functional-Oxides. *Nano Lett.* **2006**, *6*, 1535−1540.

(33) Wang, D.; Chu, J.; Liu, Y.; Li, J.; Xue, T.; Wang, W.; Qi, T. Novel Process for Titanium Dioxide Production from Titanium Slag: NaOH-KOH Binary Molten Salt Roasting and Water Leaching. *Ind. Eng. Chem. Res.* **2013**, *52*, 15756−15762.

(34) Liu, B.; Boercker, J. E.; Aydil, E. S. Oriented Single Crystalline Titanium Dioxide Nanowires. *Nanotechnology* **2008**, *19*, 505604−505610.
(35) Yuan, Z. Y.; Su, B. L. Titanium Oxide Nanotubes, Nanofibers and Nanowires. *Colloids Surf. A: Physiochem. Eng. Asp.* **2004**, *241*, 173−183.
(36) Liu, J.; Liu, Q.; Li, J.; Zheng, X.; Liu, Z.; Guan, X. Photochemical Conversion of Oxalic Acid on Heterojunction Engineered $FeWO_4$/g-C_3N_4 Photocatalyst for High-Efficient Synchronous Removal of Organic and Heavy Metal Pollutants. *J. Clean. Prod.* **2022**, *363*, No. 132527.
(37) Li, J.; Wu, X.; Pan, W.; Zhang, G.; Chen, H. Vacancy-Rich Monolayer BiO_2@x as a Highly Efficient UV, Visible, and Near-Infrared Responsive Photocatalyst. *Angew. Chem., Int. Ed.* **2018**, *57*, 491−495.

https://doi.org/10.1021/acsomega.2c02591
ACS Omega 2022, 7, 35538−35544